

## A Fabry–Perot interferometer for micrometer-sized cantilevers

B. W. Hoogenboom<sup>a)</sup>

*Institute of Physics and M. E. Müller Institute, Biozentrum, University of Basel, CH-4056 Basel, Switzerland*

P. L. T. M. Frederix

*M. E. Müller Institute, Biozentrum, University of Basel, CH-4056 Basel, Switzerland*

J. L. Yang<sup>b)</sup>

*Institute of Physics, University of Basel, CH-4056 Basel, Switzerland  
and IBM Research Division, Zürich Research Laboratory, CH-8803 Rüschlikon, Switzerland*

S. Martin, Y. Pellmont, and M. Steinacher

*Institute of Physics, University of Basel, CH-4056 Basel, Switzerland*

S. Zäch, E. Langenbach, and H.-J. Heimbeck

*FISBA OPTIK AG, CH-9016 St. Gallen, Switzerland*

A. Engel

*M. E. Müller Institute, Biozentrum, University of Basel, CH-4056 Basel, Switzerland*

H. J. Hug

*Institute of Physics, University of Basel, CH-4056 Basel, Switzerland  
and Swiss Federal Laboratories for Materials Testing and Research, EMPA, CH-8600 Dübendorf, Switzerland*

(Received 11 October 2004; accepted 21 December 2004; published online 8 February 2005)

We have developed a Fabry–Perot interferometer detecting the deflection of micrometer-sized cantilevers and other micromechanical devices, at a working distance of 0.8 mm. At 1 MHz, a noise floor of  $1 \text{ fm}/\sqrt{\text{Hz}}$  is obtained. The detector is mounted on a piezo motor for three-axis alignment. The angular alignment is not critical. The interferometer can be operated in vacuum, air, and liquid. It is particularly suited for scanning force microscopy with small cantilevers, or with larger cantilevers simultaneously monitoring vertical and lateral forces. © 2005 American Institute of Physics. [DOI: 10.1063/1.1866229]

To detect small masses, forces, and energy losses, the dimensions of silicon-based sensing devices have been reduced to the micrometer and submicrometer range.<sup>1</sup> These devices, hereafter—for convenience—denoted as “cantilevers,” allow high sensitivity and measurement speed, but also require an optimization of the detector that transforms their deflection to a macroscopic signal. In particular, small changes in position and oscillation frequency of the cantilever should be detected, without affecting its sensitivity and preferably without adding complexity to the cantilever itself. Though other deflection detectors exist, these requirements are best met using optical methods.

The most commonly used detection methods are optical beam deflection and homodyne laser interferometry; shot noise limits of below  $100 \text{ fm}/\sqrt{\text{Hz}}$  have been obtained.<sup>2</sup> However, for cantilevers with in-plane dimensions of some microns, both have their limitations. For beam deflection, a smaller spot size implies a larger optical opening angle,<sup>3</sup> and thus reduced sensitivity to changes in the angle of the deflected beam. For interferometry, the detector—typically a  $125\text{-}\mu\text{m}$ -wide fiber end with a core diameter of  $5 \text{ }\mu\text{m}$ —needs to be positioned within some microns distance from the cantilever to achieve sufficient sensitivity.<sup>4,5</sup> This is not possible when a cantilever of some microns length has to

be detected from the support chip side, as required in a scanning force microscope (SFM). This limitation can be overcome by including the interferometer cavity in the micromechanical cantilever itself,<sup>6,7</sup> or by using a heterodyne laser Doppler interferometer.<sup>8</sup>

We have preferred to minimize complexity of the cantilever and of the optical readout, and designed an interferometer with the following key features: (i) a spot size of  $3 \text{ }\mu\text{m}$ ; (ii) a detector which can be freely positioned in three-dimensional space, (iii) a convenient working distance of 0.8 mm; (iv) a sufficiently large angular alignment tolerance; (v) a finesse of 20–25, resulting in high position sensitivity; (vi) versatility, the detector is made of elements compatible with low temperature and ultrahigh vacuum, and can be operated in vacuum, gaseous, and liquid environments.

Figure 1 shows a schematic of the interferometer, as used for detecting the position of a cantilever in a SFM. Laser light ( $\lambda=783 \text{ nm}$ ) from a single-mode optical fiber passes through a lens system, which focuses the light to a  $3 \text{ }\mu\text{m}$  spot on the cantilever. To enable multiple reflections, the image distance has been made identical to the radius of curvature (0.9 mm) of the 90% reflecting lens surface (“hemi-concentric cavity”).<sup>9</sup> As a result, a reflected beam is refocused on the cantilever, even when the angle between the optical axis and the normal to the cantilever surface differs from zero. Furthermore, since the light rays are perpendicular to the lens surface (no refraction), there is no need for readjustment of the cavity when the medium between the

<sup>a)</sup>Electronic mail: bart.hoogenboom@unibas.ch

<sup>b)</sup>Present address: Institute of Semiconductors, Chinese Academy of Sciences, Qinghua Dong Lu A 35, P.O. Box 912, Beijing 100083, China

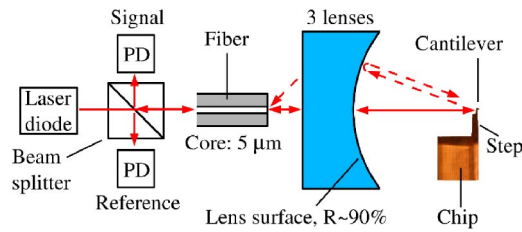


FIG. 1. (Color online) Schematic of the interferometer. The continuous arrows indicate the ideal optical path. The dashed arrows indicate the path of the first, third, ..., reflected rays in the case of angular misalignment of the cantilever.

lens surface and the cantilever (vacuum, gas, liquid) is changed. The lenses and fiber are mounted in a detector housing which can be fine-positioned along the optical axis with a piezo scanner, and aligned to the cantilever with a home-built *xyz* piezo motor of only 42 mm diameter. The backreflected intensity  $P_r$  is measured in a setup similar to Ref. 4.

To demonstrate the tolerance of the interferometer to angular misalignment, the light intensity reflected back from a macroscopic gold-coated plane mirror was measured as a function of the detector-to-mirror distance, for various mirror angles [Fig. 2(a)]. For  $0^\circ$ , sharp minima appear (finesse typically 20–25), separated by a period of half the laser wavelength ( $\lambda/2=391.5$  nm in vacuum). In this case the plane mirror surface is orthogonal to the optical axis, such that light backreflected to the fiber follows the same path as the incoming light. For nonzero mirror angles, this is only true for the zeroth, second, ... (even) rays, where the zeroth ray corresponds to the reflection back to the fiber at the first arrival at the lens surface. The first, third, ... (odd) rays couple back into the fiber under a different angle, not fully matching the numerical aperture of the fiber. The odd rays thus have a coupling factor  $T_1$  into the fiber which is differ-

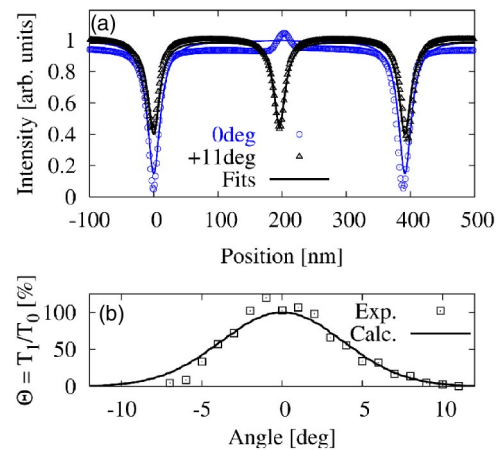


FIG. 2. (Color online) (a) Interference between the detector and a plane mirror, with the mirror roughly perpendicular to the optical axis ( $0^\circ$ ) and  $11^\circ$  rotated. The smooth curves are fits with Eq. (1). (b)  $\Theta$  derived from fits for various angles. The continuous curve is a calculation, based on the interferometer geometry, of the amount of light coupled into the fiber as a function of the mirror angle.

ent from the coupling factor  $T_0 \approx 40\%$  for the even rays.

The phase difference between two consecutive rays is  $\delta=4\pi z/\lambda$ , with  $z$  the distance between the lens surface and the plane mirror. Thus, for  $T_1=T_0$ , maximal destructive interference occurs every  $\lambda/2$ . For  $T_1 < T_0$ , odd rays can only partially interfere with even rays, and the minima become less deep. Additional minima appear, shifted by  $\lambda/4$  with respect to the main minima. For large mirror angles,  $T_1=0$ , the interference pattern is determined by the phase difference  $2\delta$  between consecutive even rays, and destructive interference occurs every  $\lambda/4$ .

The difference between  $T_0$  and  $T_1$  can be included in the standard description of a Fabry–Perot interferometer,<sup>10</sup> leading to a backreflected intensity

$$P_r = T_0 P_i \left\{ \frac{R_1 + R_1 R_2^2 + \Theta(1 - R_1)^2 R_2 - 2\sqrt{\Theta R_1 R_2(1 - R_1)(1 - R_2)} \cos \delta - 2R_1 R_2 \cos 2\delta}{1 + (R_1 R_2)^2 - 2R_1 R_2 \cos 2\delta} \right\}, \quad (1)$$

where  $\Theta=T_1/T_0$ ,  $P_i$  is the incident intensity,  $R_1 \approx 90\%$  the reflectance at the lens surface, and  $R_2$  the reflectance at the plane mirror ( $\approx 80\%$  here). Using Eq. (1) to fit interference patterns for different angles,  $\Theta$  can be obtained as a function of angle.  $\Theta$  and  $R_2$  are left free to vary,  $T_0 P_i$  and  $R_1$  are held constant for all fits. In Fig. 2(b), the resulting  $\Theta$  is shown to be in good agreement with the expected coupling to the fiber as a function of the mirror angle  $\alpha$ . For each  $\alpha$ , this coupling was calculated using the overlap integral  $\iint g(\phi - 2M\alpha, \theta)g(\phi, \theta)d\phi d\theta / \iint g(\phi, \theta)^2 d\phi d\theta$ , where  $g(\phi, \theta)$  is a Gaussian with a width derived from the numerical aperture of the fiber (0.14), and  $M=0.6$  is the magnification of the optics. For  $11^\circ$  angular misalignment (i.e.,  $T_1 \approx 0$ ) the maximum slope  $dP_r/dz|_{\max}$  and thus the deflection sensitivity are still at 60% of their value for  $0^\circ$ :  $dP_r/dz|_{\max, 0\text{deg}} \approx 0.06 \times T_0 P_i \text{ nm}^{-1} \approx 0.024 \times P_i \text{ nm}^{-1}$  (with  $P_i$  in W).

Downloaded 10 Sep 2008 to 144.82.107.152. Redistribution subject to AIP license or copyright; see <http://apl.aip.org/apl/copyright.jsp>

As a next step, the interferometer has been tested with a cantilever of dimensions  $20 \times 4 \times 0.2 \mu\text{m}^3$  and spring constant  $k=0.2$  N/m.<sup>11</sup> To enhance the reflectivity, a  $6.6\text{-}\mu\text{m}$ -long gold pad was evaporated on the end of the cantilever, using a recess step (see Fig. 1) as a shadow mask.<sup>12</sup> Making use of the geometry of the cantilever and its support chip, and of conveniently set mechanical limits of the piezo motor, the interferometer can be manually aligned to the cantilever in less than 15 min, without visual observation of the detector-cantilever alignment. In Fig. 3, the interference pattern on the cantilever is shown to be practically identical to the one obtained on a large plane mirror (i.e., the also gold-coated support chip). Using fits with Eq. (1), with  $R_2$  as the only free parameter, the reflected signal  $R_2$  from the cantilever was determined for different positions across the cantilever. When only part of the  $3\mu\text{m}$  spot falls on the cantilever,  $R_2$  rapidly drops [Fig. 3(c)].

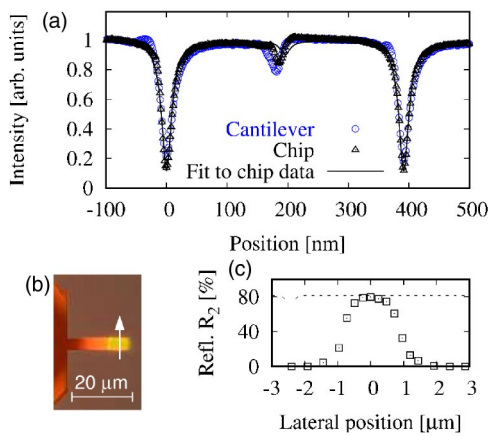


FIG. 3. (Color online) (a) Interference pattern on a gold pad at the end of a 20- $\mu\text{m}$ -long cantilever (b), compared to the interference pattern on the back of the (also gold coated) support chip, and fit with Eq. (1). (c)  $R_2$  from the fits for different positions along the arrow in (b). The dashed line indicates  $R_2$  for a large, plane mirror.

The most obvious application of the interferometer is measuring the deflection of a cantilever in a SFM. In Figs. 4(a)–4(c) we show measured thermal noise spectra of the cantilever of Fig. 3(b), in vacuum, air, and water (all at room temperature). All data were acquired without vibration isolation. Nevertheless, even at low frequencies (100 Hz) the noise is still  $\approx 10^{-12}$  m/ $\sqrt{\text{Hz}}$ , demonstrating the mechanical stability of the  $xyz$  motor. The light intensity  $P_i$  was set such that there was no sign of self-oscillation due to heating of the

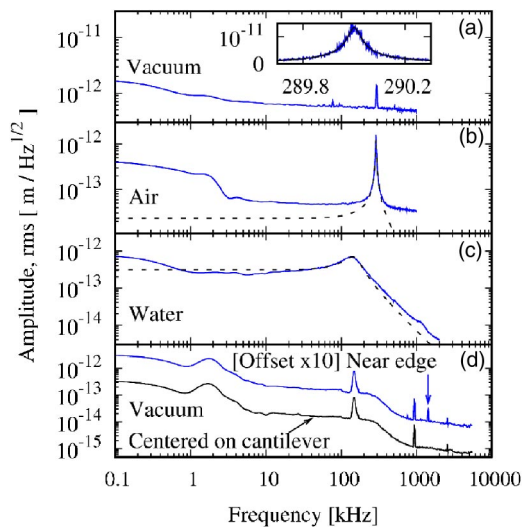


FIG. 4. (Color online) (a) Noise spectrum of a small cantilever in vacuum.  $P_i \approx 1 \mu\text{W}$ . Inset: zoom on the resonance peak at 290 kHz. The smooth line is a fit with an harmonic oscillator. (b) The same cantilever measured in air, with 10  $\mu\text{W}$ . The dashed curve is a harmonic oscillator fit around the resonance peak. (c) As (b), in water, 1 mW. (d) Noise spectrum of a conventional cantilever, 1 mW. Lower curve: detector above the main axis of the cantilever. Upper curve: detector close to the side edge of the cantilever (offset  $\times 10$  for clarity).

cantilever on any of the slopes of the interference pattern.

In Fig. 4(d) we show the thermal noise spectrum of a conventional cantilever (Nano+More GmbH,  $223 \times 31 \times 6.7 \mu\text{m}^3$ ,  $k=4 \times 10 \text{ N/m}$ , with a gold coating on the cantilever end.  $P_i$  was set at 1 mW, while it was verified that the fundamental mode did not show significant broadening compared to spectra taken at 10  $\mu\text{W}$ . Apart from the fundamental mode and higher flexural modes, the torsional mode can be observed at 1415 kHz (see arrow), depending on the lateral position on the cantilever. Note that in Fig. 4(d) the apparent height and width of the resonances are determined by bandwidth resolution and sweep time of the spectrum analyzer. In addition, we observe a broad shoulder of 20 fm/ $\sqrt{\text{Hz}}$  in Fig. 4(d) due to noise of the laser power supply (bandwidth 250 kHz), probably via wavelength variation.

Using  $dP_r/dz|_{\text{max}}$  and the detection efficiency of  $P_r$ , the shot noise limit is estimated  $\delta z_n \approx 1 \text{ fm}/\sqrt{\text{Hz}}$  for  $P_i \approx 1 \text{ mW}$ , and experimentally confirmed at 1 MHz in Fig. 4(d). For  $P_i < 0.1 \text{ mW}$ , the thermal noise  $\delta z_R$  of the preamplifier feedback resistor ( $R=100 \text{ k}\Omega$ ) is larger than the shot noise. A larger  $R$  would reduce  $\delta z_R$ , but also result in a lower measurement bandwidth (now 10 MHz). Near the cantilever resonances, in water even over a megahertz bandwidth, the thermal noise of the cantilever dominates. Reducing cantilever dimensions is one way to obtain lower cantilever noise levels. The Fabry–Perot interferometer described in this letter combines the advantages of a macroscopic interferometer (high sensitivity, versatility, and practical use) with the capability of measuring micron-sized, low-noise cantilevers.

This work was supported by the Swiss Top Nano 21 program and the NCCR Nanoscale Science. The authors acknowledge M. Despont, U. Drechsler, and P. Vettiger for their contribution to cantilever fabrication, and T. Ashworth and D. Pohl for critically reading the manuscript.

<sup>1</sup>H. G. Craighead, *Science* **290**, 1532 (2000).

<sup>2</sup>D. Sarid, *Scanning Force Microscopy* (Oxford University Press, New York, 1991).

<sup>3</sup>T. E. Schäffer, J. P. Cleveland, F. Ohnesorge, D. A. Walters, and P. K. Hansma, *J. Appl. Phys.* **80**, 3622 (1996).

<sup>4</sup>D. Rugar, H. J. Mamin, and P. Guethner, *Appl. Phys. Lett.* **55**, 2588 (1989).

<sup>5</sup>A. Oral, R. A. Grimple, H. Ö. Özer, and J. B. Pethica, *Rev. Sci. Instrum.* **74**, 3656 (2003).

<sup>6</sup>D. W. Carr and H. G. Craighead, *J. Vac. Sci. Technol. B* **15**, 2760 (1997).

<sup>7</sup>R. L. Waters and M. E. Aklufi, *Appl. Phys. Lett.* **81**, 3320 (2002).

<sup>8</sup>H. Kawakatsu, S. Kawai, D. Saya, M. Nagashio, D. Kobayashi, H. Toshiyoshi, and H. Fujita, *Rev. Sci. Instrum.* **73**, 2317 (2002).

<sup>9</sup>P. L. T. M. Frederix and H. J. Hug, (2002), patent file PCT/IB/02/03253.

<sup>10</sup>J. M. Vaughan, *The Fabry-Perot Interferometer* (Adam Hilger, Bristol, 1989).

<sup>11</sup>J. L. Yang, M. Despont, U. Drechsler, B. W. Hoogenboom, P. L. T. M. Frederix, S. Martin, A. Engel, P. Vettiger, and H. J. Hug, *Appl. Phys. Lett.* (accepted for publication).

<sup>12</sup>B. W. Hoogenboom, J. L. Yang, S. Martin, and H. J. Hug, patent file EP03025187, 2003.